Turbine mode start-up simulation of a variable speed Francis pump-turbine prototype – Part II: 3-D unsteady CFD and FEM

D. Biner[1,2], S. Alligné[3], V. Hasmatuchi[1], C. Nicolet[3], N. Hugo[4], F. Avellan[5], D. Dujic[2], C. Münch-Alligné[1]

[1] Institute of Systems Engineering, School of Engineering, HES-SO Valais-Wallis, Rawyl 47, Sion, Switzerland
[2] EPFL, Power Electronics Laboratory, Ecole Polytechnique Fédérale de Lausanne, Lausanne, Switzerland
[3] Power Vision Engineering Sàrl, St-Sulpice, Switzerland
[4] Alpiq SA, Lausanne, Switzerland
[5] EPFL, Ecole Polytechnique Fédérale de Lausanne, Avenue de Cour 33 bis, 1007 Lausanne, Switzerland

E-Mail: daniel.biner@hevs.ch

Abstract. The Z'Mutt pumping station, part of the Grande Dixence hydroelectric scheme, is one of the demonstrators of the XFLEX HYDRO project. A 5 MW reversible pump-turbine prototype equipped with a full-size frequency converter (FSFC) is used to investigate dynamic variable speed operation in pumping and generating mode. Since the FSFC converter is always connected to the electrical grid, the full rotational speed range of the motor-generator can theoretically be exploited. Furthermore, this technology enables fast operating point transitions and therefore increased grid regulation capacities. The advantages of the FSFC technology in generating mode are compared to a conventional fixed speed start-up with a variable speed start-up. The operating point trajectories are extracted from 1-D hydraulic transient simulations. Detailed hydrodynamic and structural aspects of the pump-turbine during the two start-up scenarios are further studied. Simplified unsteady 3-D CFD simulations and transient structural FEM analyses of the pump-turbine prototype are carried out to assess the harshness of the flow and to anticipate runner fatigue. The present work aims to point out potential mitigation of partial runner damages during start-up in generating mode using FSFC technology.

1. Introduction

1.1. XFLEX HYDRO project: Z'Mutt demonstrator

The increasing contribution of intermittent new renewable energy sources in today's electricity mix emphasizes the importance of balancing resources in modern power grids. The XFLEX HYDRO H2020 European Project intends to consolidate the control capacities of hydropower plants and therefore its role in future power supply systems, see [1]. The aim of the project is to demonstrate new key technologies such as smart control, variable speed hydroelectric units [2] - [5], hydraulic short circuit, and battery-turbine hybrids to finally provide a roadmap to increase the large-scale adoption of those technologies. A total of seven demonstrators at existing European hydropower plants serve as an experimental basis to assess the limits and impacts of the different flexibility technologies. The Z'Mutt

pumping station, as part of the Grande Dixence hydroelectric scheme in Switzerland, has been selected as one of the XFLEX HYDRO demonstrators. The Z'Mutt pumping station, schematized in Figure 1, is composed of five units, namely four pumps with synchronous motors of 2 x 30 MW (U1, U2) and 2 x 14 MW (U3, U4), as well as a new reversible Francis pump-turbine of 5 MW (U5), planned to be commissioned by 2021. The new pump-turbine prototype, manufactured by CKD Blansko, to be operated under a maximum gross head of 136 m will be equipped with an asynchronous motor-generator of 1000 min^{-1} nominal rotational speed, driven by a full-size frequency converter, FSFC, manufactured by ABB. The prototype will be employed in the XFLEX HYDRO experimental framework to point out the advantages and limits of high dynamic variable speed operation of reversible hydroelectric units.

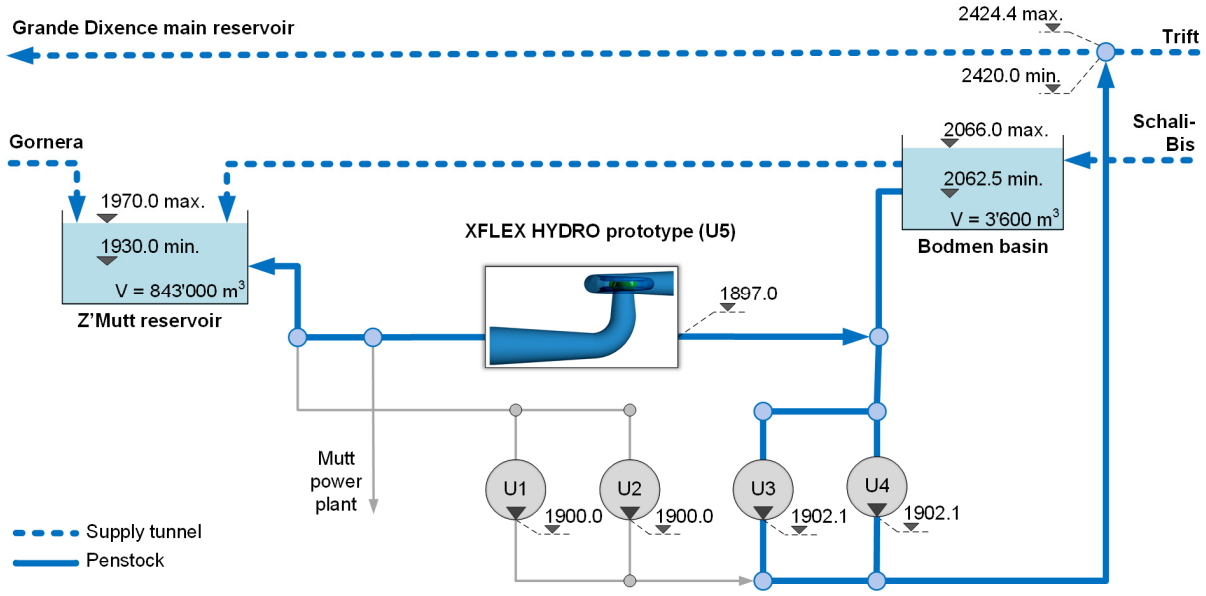

Figure 1: Schematic of the Z'Mutt pumping station.

Fast power injection or absorption, fast start and stop sequences and fast transitions between generating and pumping mode will be assessed by model tests (EPFL Technology Platform for Hydraulic Machines), 1-D transient hydroelectric simulations (Power Vision Engineering), 3-D CFD simulations and prototype field tests (HES-SO Valais-Wallis). Further, findings of the hydromechanical behavior of the new operating modes serve as an input for the adoption of new power electronic concepts (EPFL Power Electronics Laboratory) for large scale hydropower. A converter-fed synchronous machine configuration, employing a Modular Multilevel Converter, MMC, is considered as a potential future solution for variable speed technologies in large scale hydropower applications [6]. Apart from the extended capacity to provide Frequency Containment Reserve, FCR, the impact of smooth transitions on the component lifecycle, enabled by the variable speed control, is also part of the studies. The obtained findings are finally intended to be integrated into advanced control algorithms, to operate the power plant in a most advantageous way.

1.2. Investigation of turbine start-up

The aspired flexible operation of modern hydropower units may lead to increased numbers of start and stop cycles and even transitions from generating to pumping mode, related to harsh operating conditions. To avoid premature fatigue of mechanical components, these transition phases are subject to detailed investigations in the framework of the XFLEX HYDRO project. During the turbine start-up sequence, the operating point of the unit changes due to variation of rotational speed and guide vane opening. Thereby, different operating point evolutions with different durations are experienced between start-up with fixed speed technology and start-up with FSFC technology. Consequently, the damage on the unit's components may differ since it depends on the operating point and duration of the transition. Damage

contributions of fixed speed turbine start-up sequences can be mitigated by tuning the guide vane opening laws [7]. In addition to this possibility, the FSFC technology enables the precise control of the rotational speed during start-up. Thus, considering this second degree of freedom, a further reduction of partial damages is possible.

The present paper presents a preliminary numerical study of the turbine mode start-up procedure, comparing a conventional fixed speed scenario to a FSFC based variable speed scenario. Different operating points on the two start-up trajectories, extracted from 1-D transient simulations, are investigated by means of simplified unsteady CFD simulations and structural FEM analyses. Pressure fluctuations on the runner blades and mechanical torque variations are evaluated to anticipate the harshness of the flow. Finally, the unsteady pressure fields of the CFD solutions are coupled with simplified FEM analyses to assess the partial runner damage induced by each start-up trajectory.

2. Methodology

2.1. 1-D hydraulic transient simulations

As detailed in part I of this contribution, apart from the conventional fixed speed scenario, two major control strategies to start the unit with the FSFC are simulated by 1-D hydraulic transient simulations. The FSCF is either controlled by a rotational speed set point profile or an electromagnetic torque profile. It is shown that the speed control mode is safer in terms of pump-turbine transients during the start-up sequence since the operating point trajectory in the N11-Q11 frame is completely under control. Consequently, the operating point trajectories with FSFC in speed control mode is chosen to be compared with the conventional fixed speed start-up using advanced numerical simulation.

2.2. CFD simulations

The preliminary CFD investigations of the turbine start-up sequences presented in this paper are performed by means of simplified models. This methodology reduces drastically the computing time, even though the physics of the flow are not entirely captured. First, based on the steady-state assumption, a set of discrete operating points on the two start-up trajectories from the 1-D transient simulations is analysed. A total of 16 operating points is considered, 6 for the variable speed start-up, 9 for the fixed speed start-up plus the rated setpoint. Hydraulic characteristics are assumed to remain unchanged during reasonably slow transitions. For each operating point, unsteady RANS simulations with constant boundary conditions according to the 1-D results are carried out. Reduced computational domains are used to capture the main physics of the flow, as proposed by [8]. It is shown that blade torque and pressure fluctuations are underestimated using reduced numerical domains [9]. Further, the temporal accuracy of RSI effects is limited using non-uniform pitch-ratios at the rotor-stator interfaces. Furthermore, asymmetric flow phenomena in the runner domain are as well not detectable with the proposed setup. To estimate the drawbacks of the simplifications, full domain CFD computations are performed for the speed no load condition (SNL) and the rated setpoint.

2.2.1. CFD geometry and computational grids. The rotor-stator arrangement of the new pump-turbine features 10 stay vanes, 20 guide vanes and 9 runner blades. The simplified computational domain given in Figure 2 (a) (b) (c), is made of a simplified spiral casing, one stay vane channel, two guide vane channels, one runner blade channel and the full draft tube geometry with a structured mesh of 2.1 M elements. The full computational domain presented in Figure 2 (d) (e) (f) (c), features the complete spiral casing with stay vanes, the complete distributor, runner, and draft tube with a structured mesh of 12.5 M elements. A performed grid independence study confirms the actual choice of the mesh size with acceptable numerical errors on the pump-turbine performance values. Detailed information about the grid is provided in Table 1.

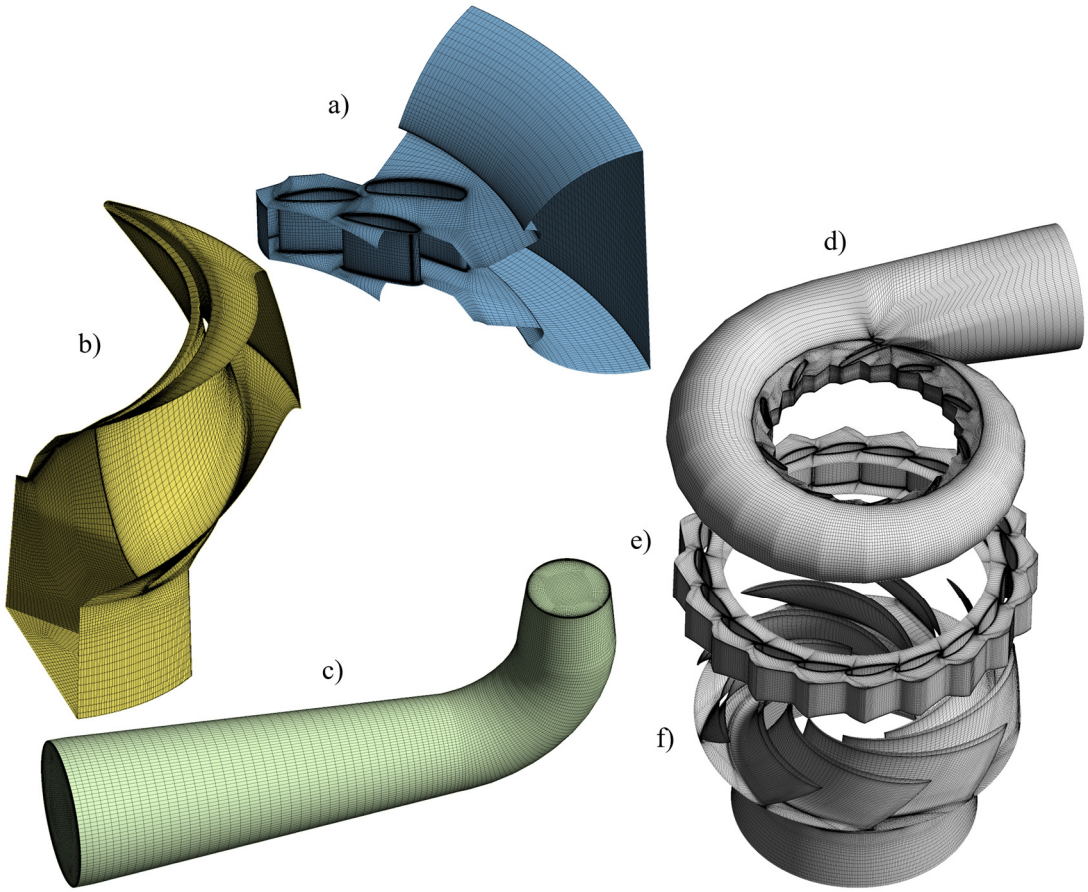

Figure 2: CFD computational grids.

Table 1: CFD grid specifications

Pos.	Description	Number of elements	Min. face angle	1st wall layer height	Max. y+	Mean y+
d)	Full spiral casing + stay vanes	2'709'256	20.2 °	75 µm - 150 µm	115.7	38.61
e)	Full distributor	2'886'240	30.8 °	50 µm - 75 µm	96.9	44.0
f)	Full runner	6'276'710	27.3 °	50 µm	111.0	45.1
a)	Partial spiral casing + stay vanes + guide vanes	822'214	33.3 °	50 µm - 150 µm	132	39.9
b)	Partial runner	684'200	27.3 °	50 µm	131.8	47.2
c)	Draft tube	595'428	42.0 °	100 µm	79.9	22.9

2.2.2. CFD boundary conditions and numerical setup. At the inlet boundary of the spiral casing, the mass flow rate is imposed with an appropriate flow direction in the case of the partial domain. The boundary condition at the draft tube's outlet is defined as opening with specified average static pressure and pressure driven flow direction. Standard periodic interfaces are defined for the reduced geometries. The rotor stator interfaces are of frozen rotor type for the steady-state flow initialization. A counter-rotating wall condition is imposed on the draft tube cone surface included in the rotating runner domain. All flow calculations presented in this paper are carried out with the commercial software ANSYS CFX R19.3, based on the finite volume method. The SST-kω turbulence model with a high-resolution advection scheme is used. The flow of each operating point is initialized by a steady-state calculation,

limiting the number of iterations to 1500 per run and using an RMS convergence criterion of 1×10^{-5}. The unsteady solution is then obtained simulating 6 runner revolutions with a typical timestep corresponding to 1.5° of rotation angle. For low rotational speeds, the maximum timestep was limited to 2×10^{-3} s. The RMS convergence criterion of 1×10^{-5} was generally achieved within the specified limitation of 10 inner iteration loops.

2.3. FEM simulations

To assess the stresses on the blade structure induced by the unsteady pressure fields, a periodic partial FEM domain is used for transient structural simulations. The periodicity imposes a cut-off for the dynamic response of the runner structure and the relevant diametrical modes of the disk-like band and crown are suppressed. Therefore, apart from the static stress component, only the response of the blade itself is accessible with the present setup. Concerning the two full CFD calculations, the pressure fields of a single blade are projected on the partial FEM domain as well.

2.3.1. FEM computational grids and boundary conditions. The FEM grid is composed of 140'500 second order tetrahedral elements with a total of 213'033 nodes. Periodicity of the grid is respected according to the cyclic boundaries. The blade thickness is discretized with at least two elements to capture the bending behaviour of the plate-like structure correctly. The critical transitions between the blade and the hub/shroud components are refined as pointed out in Figure 3. In the side-wall gaps, a linear pressure distribution law is applied with respect to static pressure at the runner inlet and outlet. A fixed support is defined at the shaft connection faces.

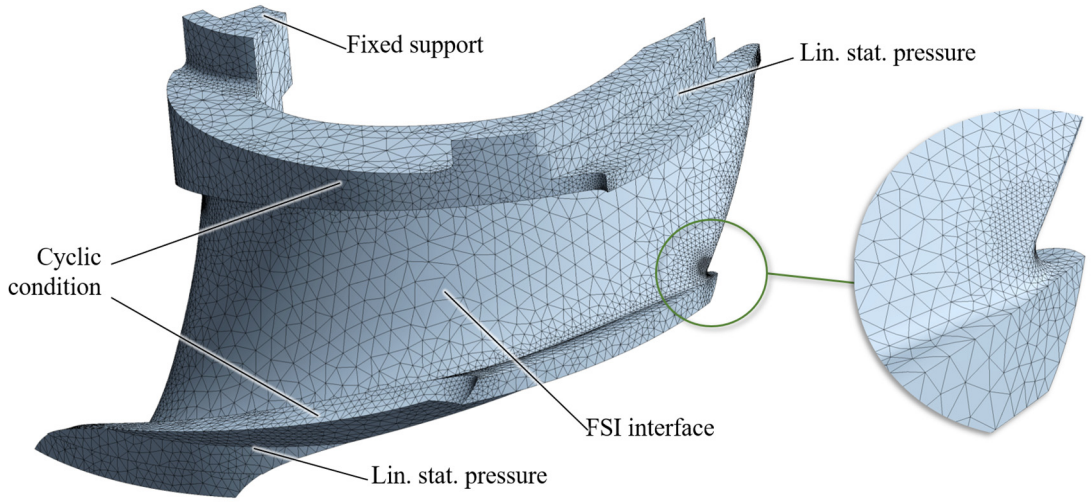

Figure 3: FEM mesh with boundary conditions.

Table 2: Material properties for FEM analyses.

Description	Symbol	Value	Unit
Tensile ultimate strength	Rm	865	MPa
Tensile yield strength	$Rp_{0.2}$	770	MPa
Poisson number	p	0.288	-
Shear modulus	G	80	GPa
Bulk modulus	K	162	GPa
Young's modulus	E	206	GPa
Density	ρ	7700	kg/m^3

2.3.2. FEM numerical setup. The transient structural FEM calculations are carried out with the commercial software ANSYS Workbench Mechanical R19.3. The properties of the material used for the analyses are given in Table 2. The time step size and simulation time frame are the same as for the CFD calculations with totally 720 time steps per operating point. Earth gravity and rotational velocity are applied to capture the mean stress level correctly. A default numerical damping value of 0.1 is used and a linear material model is considered. Loads are ramped up in a pre-load step within 1 s to initialize the simulations.

2.4. Fatigue assessments

In the framework of this preliminary work, a simplistic method is applied to anticipate the potential runner damage induced by each considered start-up sequence. For this purpose, the Von Mises stress, obtained from the FEM calculations, is used as equivalent uniaxial stress for damage calculations. The stress-life approach is based on empirical S-N curves that yield the relation between stress amplitude and the number of load cycles until initiation of critical cracks or failure of a given defect free material. Properties of fatigue design S-N curves are used according to BS 7910 [10], considering linear damage accumulation according Palmgren-Miner [11]. No endurance limit is taken into account in the present study. The total damage tally D_p of simulation point p is therefore defined as:

$$D_p = \sum_{i=1}^{I} D_{p,i} = \sum_{i=1}^{I} \frac{n_{p,i}}{C\ \Delta\sigma_{p,i}^{-3}} \tag{1}$$

The constant C depends on the quality category S-N curve and $n_{p,i}$ is the number of stress cycles with range $\Delta\sigma_{p,i}$ identified by applying a rainflow counting algorithm on the time history of equivalent stress. Furthermore, a mean stress correction according Goodman is applied:

$$\Delta\sigma = \Delta\sigma_0 \frac{Rm}{Rm - \sigma_m} \tag{2}$$

The variable $\Delta\sigma_0$ refers to the uncorrected stress range and σ_m denotes the mean value of the stress cycle. According to the simulation time frame Δt_p, the corresponding damage rate is defined as:

$$\dot{D}_p = \frac{D_p}{\Delta t_p} \tag{3}$$

Finally, the accumulated damage of each scenario is found by integration of the damage rate function $\dot{D}(t)$, obtained by a linear interpolation between the discrete, simulated values $\dot{D}_p$:

$$D = \int_{t_0}^{t_1} \dot{D}(t)\, dt \tag{4}$$

The time t_1 refers to the point where 95 % of the rated output power is achieved. The reference accumulated damage D_{ref} corresponds to the damage rate at rated operating conditions during the time frame Δt_{ref} = 1 s. Hereinafter follows the definition of the standardized, relative accumulated damage:

$$D_{rel} = \frac{D}{D_{ref}} = \frac{D}{\Delta t_{ref}\ \dot{D}_{ref}} \tag{5}$$

3. Results

3.1. CFD characteristic curves

The simulated 1-D transient and 3-D CFD operating point trajectories for both technologies, represented in the N11-Q11 and N11-T11 characteristic curves, are shown in Figure 4. The guide vane opening

values are adjusted to achieve no load conditions in the 3-D CFD simulations. The CFD results correspond to the averaged values over the three last runner rotations. Minor differences of characteristics are observed comparing the partial domain and full domain results at SNL conditions and the rated point. In terms of the N11-Q11 characteristics, the CFD results agree quite well with the predictions of the SIMSEN software. More significant deviations are observed concerning the N11-T11 trajectories. The exact source of these discrepancies is not determined at the present state.

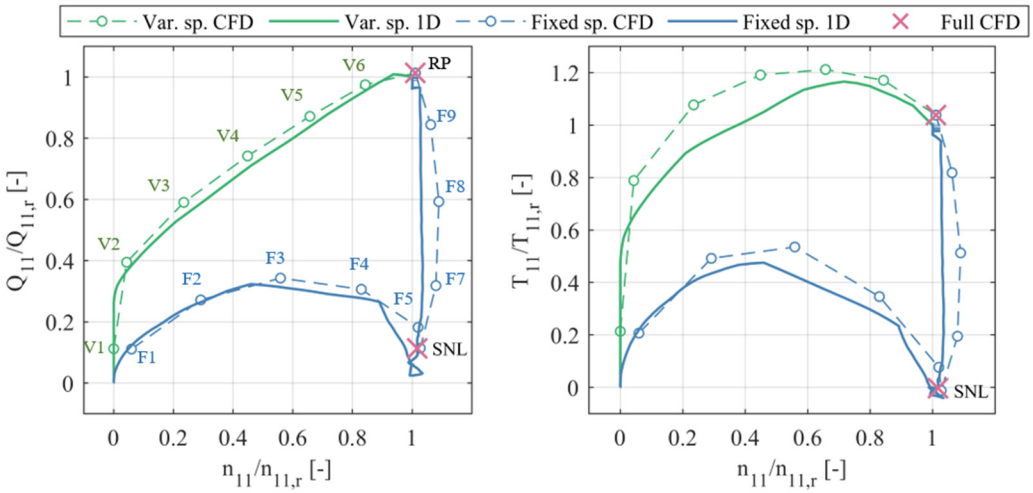

Figure 4: Simulated standardized turbine characteristics of unit 5 start-up comparing fixed speed (fixed sp.) and variable speed (var. sp.) technology.

3.2. Pressure and blade torque fluctuations

The frequency spectra obtained from CFD of the differential pressure signal between the blade pressure side and the blade suction side at three different locations in the blade middle are presented in Figure 5 where the contribution of the guide vane passing frequency f_g is indicated. The pressure fluctuations in the fixed speed case at SNL and part load conditions are distinctly more significant than during the variable speed start-up. In the starting phase of the variable speed sequence, where the runner acceleration is delayed relatively to the guide vane opening, thus, the discharge, the pressure fluctuations in the blade middle are more important than in the initial phase of the fixed speed case. The global image of the monitored pressure values lets anticipate less harsh flow conditions performing a variable speed start-up.

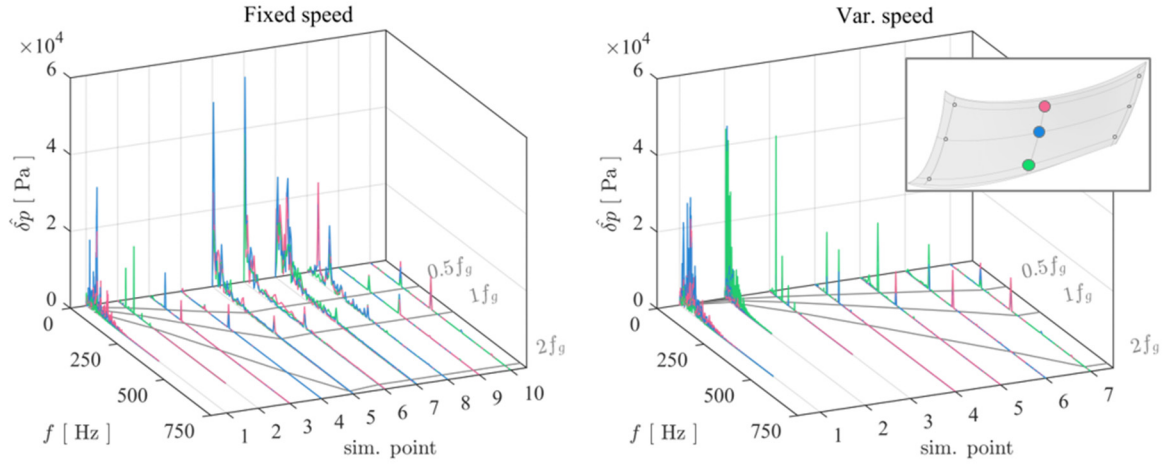

Figure 5: Spectra of simulated blade differential pressure near blade middle.

The frequency spectra obtained from CFD of the standardized blade torque signals are presented in Figure 6. The pattern of the blade torque fluctuations is similar to the image of the local pressure pulsations. Significant low frequent torque oscillations are observed during SNL and part load conditions in case of the fixed speed start-up. Further, the results of the full CFD domain simulations are indicated for the SNL condition and the rated point. Obviously, a considerable part of the low frequency content is missed at both operating points using the partial domain simulations. For example, the rotating stall phenomena cannot be captured by the simplified setup. Then, the drawback concerning the temporal accuracy using reduced runner domains is clearly visible considering the shift of the RSI peaks at guide vane passing frequency f_g.

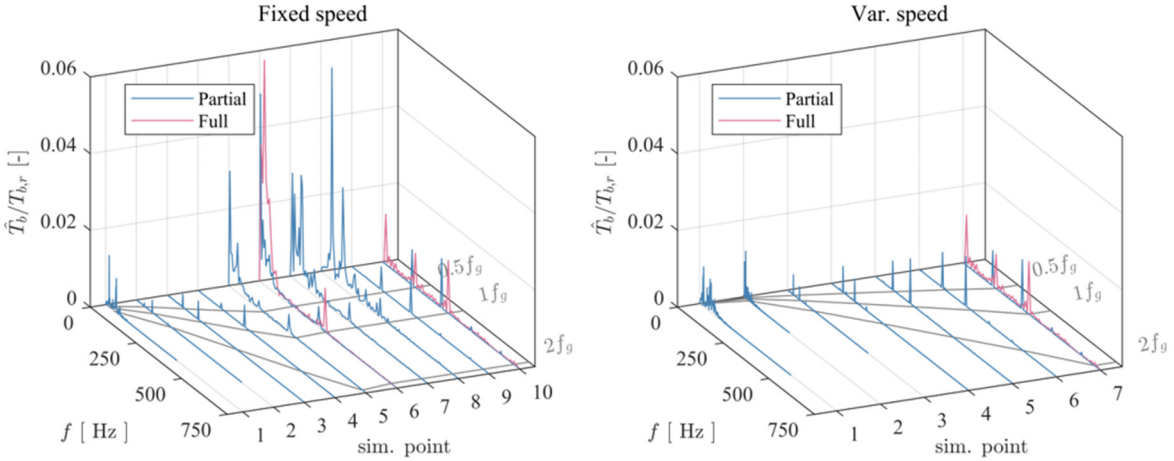

Figure 6: Spectra of simulated standardized blade torque.

3.3. Flow patterns

Instantaneous velocity streamlines in the draft tube for three selected fixed and variable speed operating points are depicted in Figure 7. The sense of rotation of the flow at the variable speed operating points is opposite to the one of the fixed speed operating points. Thus, the flow conditions during the variable speed start-up are similar to high load operation. Maximum intensity of vorticity is present at SNL conditions.

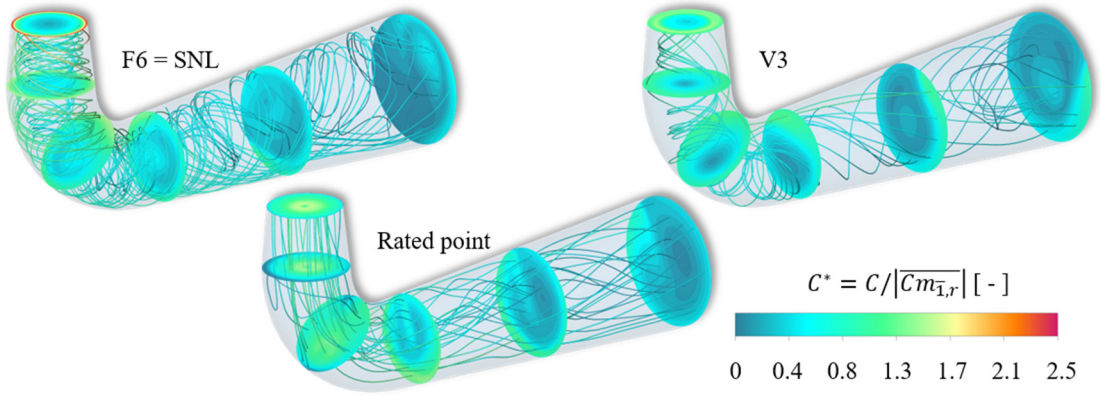

Figure 7: Instantaneous velocity streamline inside the draft tube for F6 (SNL), V3 and the rated operating point

The intensity of vortex structures inside the runner blade channel is presented in Figure 8. For the sake of illustration, two blade channels are represented (only one is simulated). A large leading edge vortex at the blade suction side occurs during the variable speed start-up. The increased stochastic pressure pulsations at the beginning of the variable speed scenario (see Figure 5) may be explained by an

instability of the leading edge vortex, whereas the flattening of the pressure amplitudes at point V3 lets anticipate a stabilization of the flow structure. Further investigations are necessary to evaluate the risk of cavitation of the leading edge vortex. A different picture is observed for the fixed speed trajectory passing from no load to the rated point. The size and number of the turbulent structures at F6, F7, and F8 indicate a stochastic nature of the flow as emphasized by the pressure spectra in the previous section. A distinct inter-blade vortex is captured at F7 that appears at the trailing edge at F8.

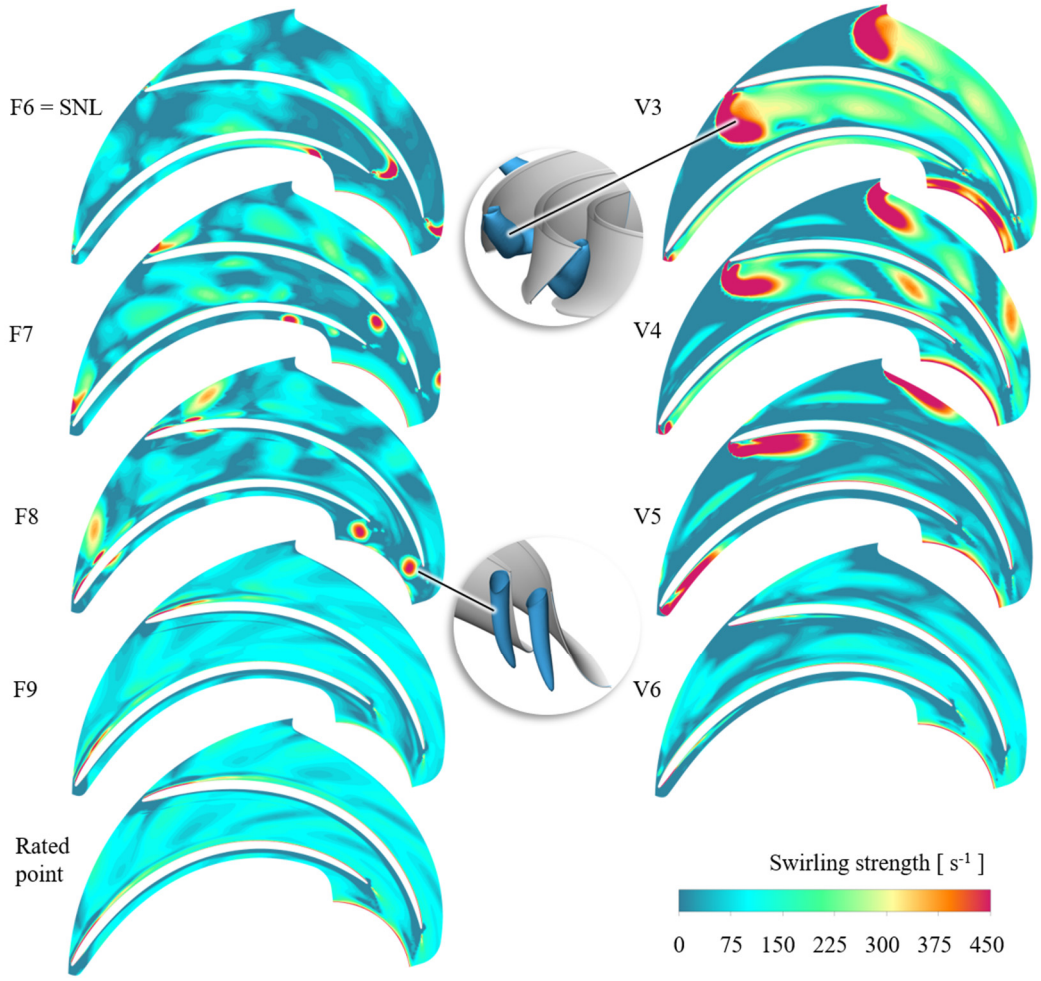

Figure 8: Instantaneous contours of swirling strength in blade channel comparing fixed and variable speed operating points.

3.4. Fatigue calculation results

The reference damage rate used for the standardization of the results is defined as the maximum damage rate detected at rated operating conditions. The evolutions of the relative damage rates are given in Figure 9. The duration to reach 95 % of the rated power is about 14 s for the variable speed case and about 36 s for the fixed speed case where an optimistic synchronisation duration of 14 s is considered. The graph represents the punctual solution at the node where the reference damage rate is defined. This location is for instance assumed critical for crack growth due to RSI dominant high cycle fatigue. In contrast to the fixed speed start-up, no excessive peak of damage rate is detected at the variable speed operating points. Furthermore, the full CFD solution projected on the simplified FEM model does not significantly change the result. Especially at the rated point, the full CFD solution leads to slightly smaller damage rates. Referring to experimental results from Lowys et al. [12], two peaks of damage rate with comparable amplitudes are measured between no load and full load conditions of a reversible

Francis pump-turbine. The first one occurs at SNL and the second one at about 50 % of the optimum power. The absence of the first damage peak in the present analyses lets anticipate that the structural response of runner band and crown is predominant concerning fatigue at SNL. In contrast, the part load instability and its impact on the runner fatigue are, to some extent, captured by the simplified models. The full FEM domain will be simulated in a next step to validate the previous statements.

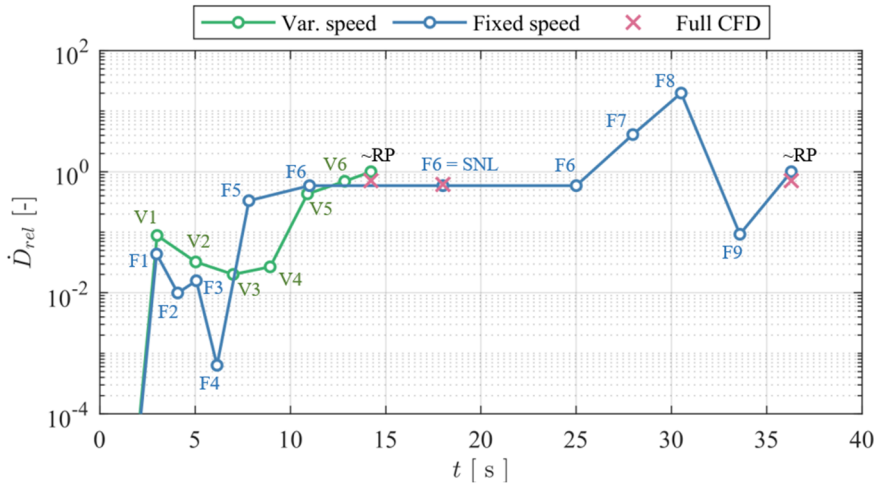

Figure 9: Evolution of relative damage rate for fixed speed and variable speed start-up.

The cumulated relative damages for the fixed speed and the variable speed scenarios are presented in Figure 10. The critical location is situated at the leading edge - shroud transition (see detail of Figure 3). According to these results, the fixed speed start-up corresponds to 107 seconds of rated operation, whereas the variable speed start-up corresponds to 3.58 s of rated operation. Despite the simplified models, the present preliminary study lets anticipate a considerable potential to mitigate partial damages during turbine start-up using the FSFC technology by a factor of $107 \div 3.58 \approx 30$. More sophisticated turbulence models and more complete structural models will be applied in the next steps prior to the prototype field test planned for end of 2021. The experimental data will be crucial to evaluate the validity of the numerical approaches and to bring the evidence of fatigue damage mitigation adopting FSFC technology.

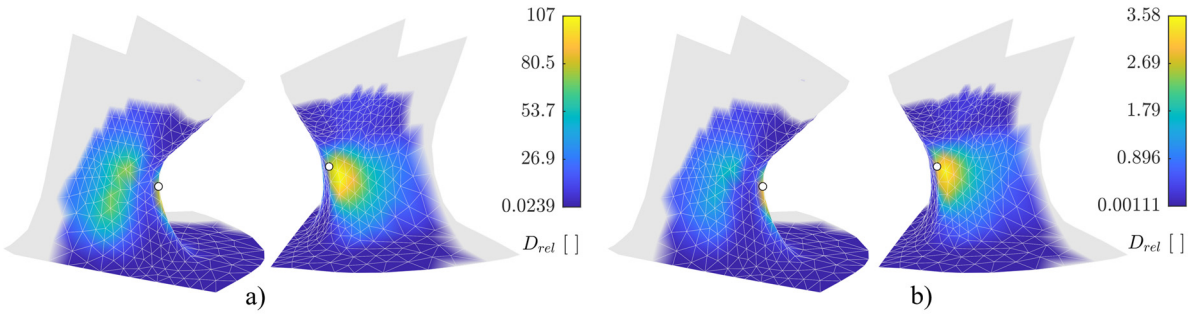

Figure 10: FEA results of accumulated relative damage during fixed speed start-up (a) and variable speed start-up (b) at critical blade location.

4. Conclusion

A preliminary numerical study of the turbine mode start-up procedure of a 5 MW Francis pump-turbine prototype comparing fixed speed and variable speed technologies is performed. Based on 1-D simulation results, a set of discrete operating points on the fixed speed and variable speed start-up trajectories are defined to evaluate the flow conditions inside the pump-turbine by means 3-D CFD simulations. CFD results show that pressure fluctuations on the runner blade are significantly reduced using FSFC

technology. A distinct leading edge vortex is observed at the variable speed operating points that is subject to further investigations and optimization of the turbine start-up procedure. Then, a simplified one way coupled FSI analysis is carried out to assess runner blade damage induced by the start-up process. According to the present simplified numerical analyses, the accumulated partial damage is approximately 30 times lower using the FSFC technology. A significant damage peak is detected during the fixed speed start-up at about 60 % of the rated power that is in good agreement with results from literature. In contrast, the expected damage peak at SNL conditions remains unidentified. Since the full CFD solution applied to the simplified FEM model does not significantly increase the damage rate at SNL, it is supposed that the suppressed dynamic behaviour of the runner band and crown is responsible for the incomplete image. Therefore, full FEM models need to be considered in a next step for a more complete understanding of the fatigue mechanisms. Nevertheless, the first insights presented in this paper let anticipate a considerable potential to increase the lifetime of pump-turbine units adopting FSFC technology.

5. Acknowledgements

The Hydropower Extending Power System Flexibility (XFLEX HYDRO) project has received funding from the European Union's Horizon 2020 research and innovation programme under grant agreement No 857832. The authors would like to thank CKD Blansko and Hydro Exploitation SA for their collaboration and support.

References

[1] https://xflexhydro.net/

[2] T. Kuwabara, A. Shibuya, H. Furuta, E. Kita, K. Mitsuhashi, Design and Dynamic Response Characteristics of 400 MW Adjustable Speed Pumped Storage Unit for Ohkawachi Power Station, IEEE Transactions on Energy Conversion, Vol. 11, Issue 2, pp. 376-384, June 1996.

[3] E. Kopf, S. Brausewetter, M. Giese, F. Moser, Optimized control strategies for variable speed machines, In Proceeding of the 22nd IAHR Symposium on Hydraulic Machinery and Systems, Stockholm, Sweden, June-July 2004.

[4] Y. Pannatier, B. Kawkabani, C. Nicolet, J.-J. Simond, A. Schwery, P. Allenbach, Investigation of control strategies for variable speed pump-turbine units by using a simplified model of the converters, IEEE Transactions on Industrial Electronics, Vol. 57, Issue 9, 2010, pp: 3039-3049.

[5] J. Hell, M. Egretzberger, A. Lechner, R. Schürhuber, Y. Vaillant, Full size converter solutions for pumped storage plants – a promising new technology, Hydro 2012, Euskalduna Congress Centre Bilbao, Spain, 29-31 October 2012.

[6] M. Basic, P. Silva, D. Dujic, High Power Electronics Innovation Perspectives for Pumped Storage Power Plants, Hydro 2018, Gdansk, Poland, 2018.

[7] J. Löfflad, M. Eissner, Lifetime assessment and plant operation optimization based on geometry scan and strain gauge testing – START/STOP optimization, 10th International conference on hydraulic efficiency measurements, Itajuba, Brazil, 2014.

[8] J. Nicolle, A.M. Giroux, J.F. Morisette, CFD configurations for hydraulic turbine startup, IOP Conf. Series: Earth and Environmental Science, IOP Publishing, 2014, Vol. 22, 032021.

[9] J. Nicolle, S. Cupillard, Prediction of dynamic blade loading of the Francis-99 turbine, Journal of Physics: Conference Series 579, 2015, 012001.

[10] BSI, BS 7910:2013+A1:2015 - Guide to Methods for Assessing the Acceptability of Flaws in Metallic Structures, BSI, 2013.

[11] A. Nussbaumer, L. Borges, L. Davaine, Fatigue Design of Steel and Composite Structures: Eurocode 3: Design of Steel Structures, Part 1-9 Fatigue, John Wiley & Sons, 2012.

[12] P.-Y. Lowys, F. André, F. Duparchy, R. Guillaume, J. C. Ferreira, A. F. da Silva, "Alqueva l and Salamonde ll: A new approach for extending turbine operation range," Hydro 2014, 2014.